

## Vibration analysis of CFST tied-arch bridge due to moving vehicles

Jian-Rong Yang\*<sup>1</sup>, Jian-Zhong Li<sup>2</sup> and Yong-Hong Chen<sup>3</sup>

<sup>1</sup>*Faculty of Civil Engineering and Architecture, Kunming University of Science and Technology, Kunming 650051, China*

<sup>2</sup>*Department of Bridge Engineering, Tongji University, Shanghai 200092, China*

<sup>3</sup>*Kunming Metallurgy College, Kunming 650033, China*

*(Received July 9, 2010, Accepted October 25, 2010)*

**Abstract.** Based on the Model Coupled Method (MCM), a case study has been carried out on a Concrete-Filled Steel Tubular (CFST) tied arch bridge to investigate the vibration problem. The mathematical model assumed a finite element representation of the bridge together with beam, shell, and link elements, and the vehicle simulation employed a three dimensional linear vehicle model with seven independent degrees-of-freedom. A well-known power spectral density of road pavement profiles defined the road surface roughness for Perfect, Good and Poor roads respectively. In virtue of a home-code program, the dynamic interaction between the bridge and vehicle model was simulated, and the dynamic amplification factors were computed for displacement and internal force. The impact effects of the vehicle on different bridge members and the influencing factors were studied. Meanwhile the acceleration responses of some of the components were analyzed in the frequency domain. From the results some valuable conclusions have been drawn.

**Keywords:** vibration; tied-arch bridge; vehicle-bridge interaction; amplification; hanger.

---

### 1. Introduction

Today there is a constant demand for increasing the allowable axle loads, speed and number of heavy vehicles to make highway transportation more competitive. Meanwhile advanced materials and improved design methods have resulted in lighter and more flexible bridges. Therefore highway bridges are increasingly susceptible to vibration. Vibration of large amplitude may introduce into the bridges structural damage and increase their retrofitting expenses. Damage in some local elements of bridge, such as deck slabs, hangers and expansion joints, could be dangerous to highway transportation. Thus the research on local vibration of highway bridges becomes a necessity.

Most of the recent studies focus mainly on beam type bridges, among which plan frame element is usually applied to build bridge models. But this type of model makes too many simplifications to accurately describe the dynamic characteristics of the structures, especially those whose vibration is governed by more than one mode (e.g. arch bridge, cable stayed bridge, curved and skew bridge).

---

\* Corresponding author, Ph.D., Associate Professor, E-mail: [carpenter\\_y@sina.com](mailto:carpenter_y@sina.com)

Inspired by a series of accidents of structural failure (Lu 2005), the dynamic behavior of tied-arch bridge due to heavy vehicle loads has become an interesting subject since recently.

The Concrete-Filled Steel Tubular (CFST) tied-arch bridge is more competitive than other tied-arch bridges in china for their lower building cost, lower demands on soil foundation, and convenience of constructing. However, the design theory for CFST tied-arch bridges has been far behind their engineering practice, and after decades of operation, some of them are subject to damages induced by traffic loads. Many researchers have committed themselves to the investigation of vehicle induced vibration of CFST tied-arch bridge and obtained some valuable results. Wu *et al.* (2003) studied the vehicle-bridge dynamics characteristic of Nielsen arch bridge in high speed railway, and compared the difference between the *X* style arch and the parallel arch in the bridge. Shan *et al.* (2005) evaluated the vertical and transverse displacements of *X* style arch bridge, its dynamic amplification factor, and the offload factors of vehicles. Roeder (2000) conducted an on-the-spot experiment research on a steel tied-arch bridge, and reported the measured DAF varied between 0.9-1.7 for the floor beams, 0.6-1.1 for the stringers, 0.94-1.35 for arch rib and hangers. Li *et al.* (2003) carried out a model test on a Nielsen *X* style CFST tied-arch bridge, and thoroughly studied the force distribution and loading resisting capacity of this type of structure. Malm (2006) performed field testing and simulation of a tied-arch bridge, and studied the fatigue in various structural components according to the Palmgren-Miner's rule. The measured data results were compared with those from the FE model to give a better understanding of the dynamic behavior of the bridge.

Finite element analysis of large bridges usually demands large computation scale. Generally the higher order modes are in the absolute predominance, while the lower order modes play an less important role in bridge local dynamic response. In order to obtain the higher order modes, elements for the structure should be meshed with the smallest possible size. Therefore the computing and post-process procedure may become intolerably tedious. The Model Coupled Method (MCM) (Henchi 1998) is an effective algorithm developed for the resolution of vehicle-bridge interaction problem. The method uses a modal superposition technique for the bridge or the vehicle, and gives a unique coupled system by eliminating the interaction forces between the two subsystems. Thus the degrees-of-freedom of the coupled system, and the CPU time as well, can be greatly reduced. Some other advantages of the MCM can be quoted as: easy and compact numerical implementation, reduced computer memory storage, no factorization of the global matrix, and no iteration in the computational process.

The primary objective of this study is to investigate the vehicle induced vibration of CFST tied-arch bridge. Based on MCM, the equations of motion of the coupled road vehicle-bridge system are established and solved by the Wilson- $\theta$  method. A comprehensive computer program is accordingly developed. The dynamic responses of the bridge, such as displacement, acceleration and internal force are computed and discussed in detail. The results obtained provide a background for verification and modification of design and evaluation specifications of highway bridges.

## 2. Vehicle and bridge model

### 2.1 Vehicle model

In establishing a mathematical model to represent the vehicle dynamics, the following assumptions are made: (1) vehicle bodies are rigid; (2) the wheels maintain full contact with the

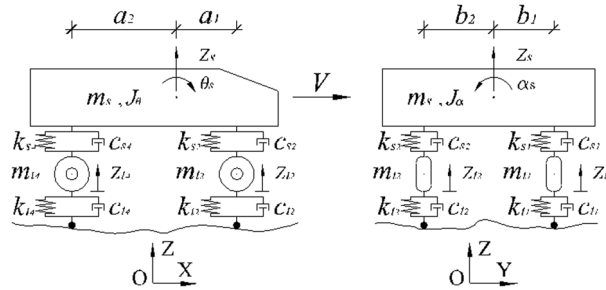


Fig. 1 Three dimensional vehicle model of seven degrees-of-freedom

bridge surface without separation; (3) all springs are linear, and damping is viscous; and (4) all rigid bodies have small displacements about their static equilibrium position (Zhang 2006).

As shown in Fig. 1, the vehicle model is composed of one vehicle body and four wheel bodies. The tires and suspension systems are idealized as linear elastic spring elements and dashpots. The vehicle body has three degrees-of-freedom, including  $z$  displacement, rolling, and pitching; each wheel has only one degree-of-freedom, namely  $z$  displacement. Therefore, each vehicle has a total of seven degrees-of-freedom.

In the analysis, the mass of vehicle body  $m_s = 25.5$  t; the pitching ( $J_\theta$ ) and rolling ( $J_\alpha$ ) moment of inertia of vehicle body are  $55.3 \text{ t} \cdot \text{m}^2/\text{rad}$  and  $56.89 \text{ t} \cdot \text{m}^2/\text{rad}$  respectively; the damping coefficients of vehicle suspension ( $c_{s1}, c_{s2}, c_{s3}, c_{s4}$ ) are 20.0 kNs/m; the spring stiffness coefficients of vehicle suspension for the front ( $k_{s1}, k_{s2}$ ) and rear ( $k_{s3}, k_{s4}$ ) axles are 4.00 and 8.00 MN/m respectively; the mass of each front axle tires is 445 kg, and each rear axle tires is 890 kg; the damping coefficient for each tires ( $c_{t1}, c_{t2}, c_{t3}, c_{t4}$ ) is 20.0 kNs/m; the spring stiffness coefficients of tires for the front ( $k_{t1}, k_{t2}$ ) and rear ( $k_{t3}, k_{t4}$ ) axles are 2.25 and 8.00 MN/m respectively; the distances  $\alpha_1, \alpha_2, b_1,$  and  $b_2$  are 3.479, 1.021, 0.915, 0.915 m respectively (Fafard 1998). The seven natural frequencies of the vehicle are calculated with the Stodola method (Bhatt 2002), which are 2.03, 3.22, 4.27, 18.91, 19.77, 21.41 and 21.63 Hz respectively.

## 2.2 Bridge model

In order to obtain representative results, the general structural arrangement was determined according to the design of similar bridges (Chen 2002). The bridge is a through tied-arch bridge with CFST arch ribs. It is 90 m long and 20.7 m wide, with 13 bays in the arch and floor system. The arch ribs are shaped into an inversed catenary with  $m = 1.1$ , a rise-span ratio 1/5, and connected by 5 braces. The depth of the main arch rib is 2300 mm. The cross-section of the two main arch ribs comprises dumbbell-type concrete-filled steel tubes with the dimensions of 900 mm  $\times$  14 mm and C50 expansive concrete filled. There are 12 hangers made of 109  $\phi$  7 high strength steel wire on each side of the bridge. They are numbered from 1 to 12 where hangers 1 and 12 are the shortest and hanger 6 is the longest. The main arch ribs are connected individually by eight pre-stressed strands on each side in the longitudinal direction, which act as tie bars and were pre-stressed by 11200 kN force. The floor system consists of a 330 mm thick concrete slab supported directly by cross beams at a spacing of 6.9 m.

A three dimensional finite element model (FEM) is developed for the bridge in the general

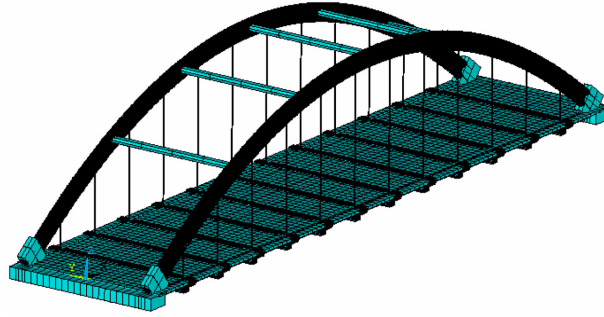


Fig. 2 Finite element model of the bridge

commercial FE package ANSYS as shown in Fig. 2. The arch ribs are composed of steel tube and concrete which is supposed to work together. Therefore the steel tube and its filled-in concrete are represented separately as two-node beam elements (BEAM44) which share the same group of nodes. The beams (both transverse and longitudinal), hangers, and braces are modelled as beam elements (Beam44). The deck slab was modelled using shell elements (SHELL43). The two supports of each rib are connected horizontally by link elements (LINK8) to model the tie chords.

Based on the design documents from the manufacturer, the mass per meter of the hangers and tie rods is 1.2 times higher than those of their steel cables alone. Accordingly the mass of elements for hangers and tie rods is multiplied 1.2 times. Considering the effects of gravity stiffness of the hangers, analysis is done on two bridge models, in which the boundary condition of the hangers is simulated as hinged and fixed respectively.

### 3. Vehicle-bridge interaction

#### 3.1 Vehicle-bridge model

The modal equations of a bridge can be expressed as

$$[M_B]\{\ddot{A}\} + [C_B]\{\dot{A}\} + [K_B]\{A\} = \{F_B\} \quad (1)$$

where  $\{A\}$  = modal displacement vector;  $[M_b]$  = modal mass matrix;  $[C_b]$  = modal damping matrix; and  $[K_b]$  = modal stiffness matrix of the bridge;  $\{F_b\}$  = modal wheel-bridge contact force vector on the bridge. The equations of motion for the vehicle model presented in Fig. 2 are derived via the Lagrange's formulation as

$$[M_V]\{\ddot{Z}\} + [C_V]\{\dot{Z}\} + [K_V]\{Z\} = \{F_V\} \quad (2)$$

where  $\{F_V\}$  is the contact force vector applied on the vehicle;  $[M_V]$ ,  $[C_V]$  and  $[K_V]$  are, respectively, the mass, damping and stiffness matrices of the vehicle;  $\{Z\}$  is the vertical displacement vector of the vehicle.

#### 3.2 Interaction of vehicle and bridge

The interaction force between the bridge and the vehicle on the  $i$ th wheel is given by

$$F_{ti} = -k_{ti}(Z_{ti} - U_{bi} - r_i) - c_{ti}(\dot{Z}_{ti} - \dot{U}_{bi} - \dot{U}'_{bi}V - \dot{r}'_iV) \tag{3}$$

where:  $k_{ti}$  and  $c_{ti}$  are, respectively, the tire stiffness and tire damping of the  $i$ th wheel;  $Z_{ti}$  is the vertical displacement of the  $i$ th wheel;  $U_{bi}$  and  $r_i$  are, respectively, the bridge vertical displacement and the road surface roughness under the  $i$ th wheel; and  $V$  is the speed of the vehicle.

Based on the  $j$ th modal displacement under the  $i$ th wheel  $\phi_j^i$ ,  $U_{bi}$  can be expressed with modal linear superposition technique as

$$U_{bi} = \sum_{j=1}^N \phi_j^i A_j \tag{4}$$

where  $N$  = dimension of the modal space. The force acted on bridge deck by the  $i$ th wheel is expressed as  $F_{bi} = F_{Gi} - F_{ti}$ , in which  $F_{Gi}$  is the vehicle gravity under the  $i$ th wheel. While the  $n$ th to  $m$ th wheels of the vehicle are located on the deck, the  $L$ th modal force in Eq. (1) can be derived as

$$F_{BL} = \sum_{i=n}^m \phi_L^i F_{bi} \tag{5}$$

Substituting Eq. (5) into Eq. (1) for all modes, then it becomes

$$\begin{bmatrix} [M_V] & [0] \\ [0] & [M_B] \end{bmatrix} \begin{Bmatrix} \{\ddot{Z}_V\} \\ \{\ddot{A}\} \end{Bmatrix} + \begin{bmatrix} [C_V] & [C_{Bt}] \\ [C_{Bt}]^T & [C_B + C_{BV}] \end{bmatrix} \begin{Bmatrix} \{\dot{Z}_V\} \\ \{\dot{A}\} \end{Bmatrix} + \begin{bmatrix} [K_V] & [K_{Bt1}] \\ [K_{Bt2}] & [K_B + K_{BV}] \end{bmatrix} \begin{Bmatrix} \{Z_V\} \\ \{A\} \end{Bmatrix} = \{F\} \tag{6}$$

where the additional terms  $C_{Bt}$ ,  $C_{BV}$ ,  $K_{Bt1}$ ,  $K_{Bt2}$  and  $K_{BV}$  are due to the contact force. They are all functions of bridge properties, vehicle properties and the positions of vehicle-bridge contact points. This indicates that the additional terms in Eq. (6) are time-dependent and will change as the vehicle moves along on the bridge.

### 3.3 Road surface roughness

A vehicle travelling over a bridge and its approach roadways which containing surface irregularities experiences vertical and horizontal motions. These motions create additional forces in addition to the vehicle load. They depend on the suspension characteristics and the moving speed of vehicle, and the condition of pavement. The typical road profile may be described by a periodically modulated random process. One method of characterizing a random function is to use the Power Spectral Density (PSD) function. Dodds and Robson (1973) developed a typical PSD function that can be approximated by exponential functions as

$$S(f) = \begin{cases} S(f_0)(f/f_0)^{-\alpha_1}, & f \leq f_0 \\ S(f_0)(f/f_0)^{-\alpha_2}, & f \geq f_0 \end{cases} \tag{7}$$

where  $S(f)$  = PSD function ( $m^2/cycle/m$ ) for road surface elevation;  $f$  = wave number (cycle/m);  $f_0$  = discontinuity frequency (cycle/m,  $1/2\pi$ ); the values of  $\alpha_1$ ,  $\alpha_2$  are taken as 2 and 1.4, respectively;  $S(f_0)$  = roughness coefficient ( $m^2/cycle/m$ ), and its value is chosen depending on the road condition. The profiles modelled as a stationary Gaussian random process can be generated by an inverse Fourier Transform as follows

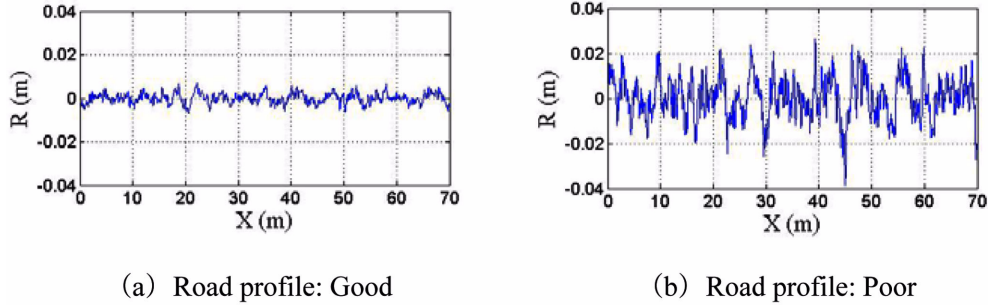


Fig. 3 Road profile with road roughness

$$R(x) = \sqrt{2} \sum_{k=1}^N \sqrt{S(f_k) \Delta f} \cos(2\pi f_k x + \theta_k) \quad (8)$$

where  $R(x)$  = road profile (m);  $S(f_k)$  = PSD function ( $\text{m}^2/\text{cycle}/\text{m}$ );  $f_k$  = wave number/spatial frequency (cycle/m);  $\Delta f$  = sampling bandwidth of spatial frequency (cycle/m);  $\theta_k$  = random figure uniformly distributed in  $[0, 2\pi]$ ;  $N$  = number of sampling frequencies. In this paper, the values of 0, 16, 256 ( $10^{-6} \text{ m}^2/\text{cycle}/\text{m}$ ) are used according to the ISO specifications (ISO 1995), as the roughness coefficients for the class of Perfect, Good, and Poor roads respectively. The generated sample road profiles with road roughness are shown in Fig. 3.

In the present study, the random road surface roughness profiles were generated once and then used for all calculations. This approach excludes the uncertainty of surface roughness (because each run could generate a different profile) for the comparison study.

## 4. Numerical results

### 4.1 Frequencies of free vibration

A total of 300 modes are computed by subspace iteration method. The two bridge models with different boundary conditions of the hangers have almost identical modal shapes. When the hangers are fixed at both ends, vibration frequencies of the bridge appear slightly higher than the model with hangers hinged at both ends. The first vibration mode is symmetric transverse bending of the main arches with a frequency of 0.4610 Hz. This matches the common feature that, for CFST tied-arch bridges, the in-plane stiffness of the arch ribs is superior to that of out-of-plane. The second mode is vertical anti-symmetric bending in 0.9447 Hz. Since the deck and arch ribs are connected with flexible hangers, they can be regarded approximately as independent structures in plane. This is characterized by non-synchronous vibration in their modal shapes. Usually the vibration of the deck lags behind that of the arch ribs. Hence the deck slabs of some bridges will experience excessive vibration under passing vehicles. In the light of this, the stiffness of deck system should be appropriately increased to reduce or even eliminate the vibration.

The hangers have higher natural frequencies in the longitudinal direction due to the higher degree of restraint in the connection with the main arches and transverse beams. Since the hangers have

Table 1 Natural frequencies of the hangers

Hanger	1	2	3	4	5	6
Length (m)	5.172	9.446	12.841	15.374	17.056	17.895
Tension (N)	1.0040e6	1.0776e6	1.0486e6	1.0425e6	1.0422e6	1.0428e6
	Theory					
$f$ (Hinged, Hz)	19.4468	11.1961	8.3312	7.0422	6.4040	6.1324
$f$ (Fixed, Hz)	22.4749	12.9313	9.6213	8.1323	7.3952	7.0815
	ANSYS					
$f$ (Hinged, Hz)	19.4649	11.2081	8.3404	7.0501	6.4113	6.1395
$f$ (Fixed, Hz)	20.4626	11.7661	8.7535	7.3987	6.7280	6.4427

Note: since the bridge is symmetric, frequencies of only half span are listed.

different lengths and axial pre-stresses, their natural frequencies differ from each other. For the hinged hangers, the  $n$ th natural frequency  $f_n$  can be expressed as follows (Li 1996)

$$f_n = n^2 \pi / 2l^2 \sqrt{E(I + Sl^2 / n^2 \pi^2 E)} / m \tag{9}$$

where  $E$  = the Young's modulus of material;  $I$ ,  $l$ , and  $m$  are section moments of inertia, length of hanger, and mass per unit length of the hanger, respectively;  $S$  = the tension existing in the hanger. And for the fixed hangers, their natural frequencies can only be obtained by solving a transcendental equation. Song (2001) suggested a simplified form to approximate the fundamental frequencies  $f$  as

$$f = 2 \pi / \sqrt{3} l^2 \sqrt{E(I + Sl^2 / 4 \pi^2 E)} / m \tag{10}$$

Summarized in Table 1 are the natural frequencies of all hangers with both ends fixed and hinged, which are obtained from the theoretical formulas (Eq. (9) and Eq. (10)) and from ANSYS, respectively. For the hinged hangers the results from both Eq. (9) and ANSYS are consistent with each other; but for the fixed hangers the results differ slightly by reason of approximation made by Eq. (10).

Though the boundary conditions of the hangers have little effect on the fundamental frequency of the bridge, the results in Table 1 reveal that: the natural frequencies of hangers with both ends fixed are much higher than those of the hinged hangers on the condition that the length and axial pre-stress remain equal.

#### 4.2 Dynamic amplification effects

When the dynamic characteristics of the system are obtained, the vehicle-bridge interaction process is simulated with MCM. The modal damping ratio of each mode is taken as constant deliberately  $\xi = 0.03$ . Initially both the vehicle and bridge are assumed to be at rest, and the vehicle travels forward at a uniform speed, with a 20 m leading distance to minimize the effect of initial conditions on bridge vibration. The same class of road surface roughness is assumed for both the approach roadway and bridge decks. And road profile remains fixed along the transverse direction. Three vehicle lanes, TR1, TR2, and TR3, are considered to determine the maximum traffic action

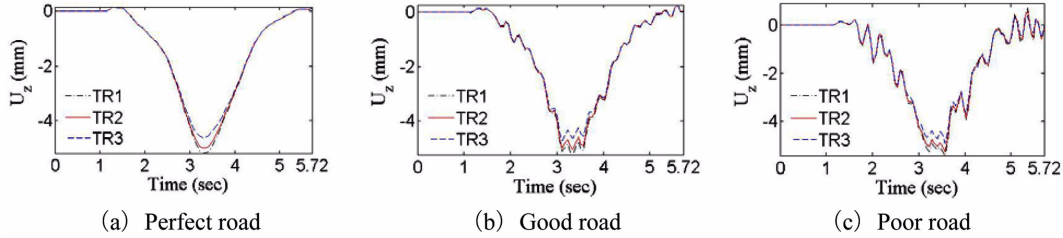
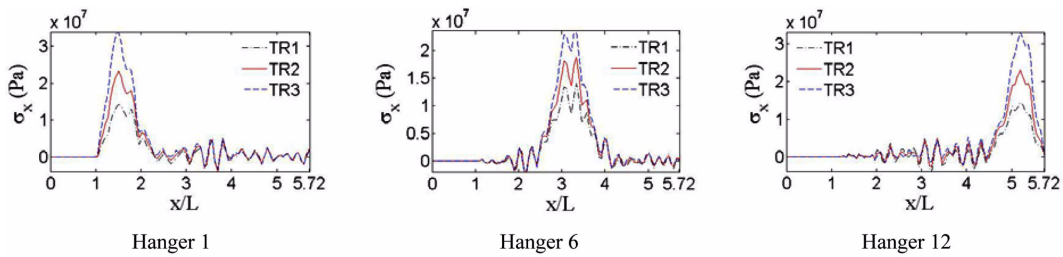
Fig. 4 Vertical displacement of middle span slab ( $V = 20$  m/s)

Fig. 5 Axial force time histories of the hangers

effects. They are all parallel to the center line of the bridge and drift off the line by 0, 3.6, and 7.2 m respectively. Vehicle speeds ranging from 10 to 40 m/s are considered, which cover the speed limit of most highways. In order to scan the road profile correctly and to avoid convergence problems, the time steps are relatively short, thus in all runs, the vehicle progressed over the bridge in steps of 0.005 m. Therefore each simulation requires 22,900 steps.

The dynamic displacements in vertical direction are computed for the arch ribs, slabs, and hangers respectively. The displacement value  $U_z$  is measured upwards from the original position of structure if  $U_z$  is positive or downwards if  $U_z$  is negative. The typical displacement time histories of middle span slab at a vehicle speed of 20 m/s are shown in Fig. 4. The simulations are carried out for three different road surface profiles with the vehicle passing along different lanes. The figure shows that the dynamic response curves fluctuate near the corresponding influence lines, considering the effects of vehicle mass, speed, road surface profile, and lane. The highest displacements occur for the Poor road surface profile. At each data point, the extreme dynamic and static displacements correspond to the same critical lane.

The dynamic axial stress response can be computed for each hanger. Based on the variation of axial stress the stress amplitude is obtained accordingly. In Fig. 5, the typical axial stress time histories of the hangers with both ends fixed are shown. The simulations are carried out for Good road with the vehicle passing along different lanes at a speed of 20 m/s. Fig. 5 shows that the axial stress of each hanger varies according to vehicle position, and reaches the peak value when the vehicle approaches. And the dynamic peak values are higher than those of static ones. This illuminates that the hangers are mainly subject to local impact of the vehicle. In safety evaluations the dynamic effect is taken into account by a so-called dynamic amplification factor (DAF).

Typical DAF is usually expressed as the ratio of maximum dynamic response  $R_D$  to maximum static response  $R_S$ :  $DAF = R_D/R_S$ . In this study DAFs are calculated for vertical displacement,

Table 2 Maximum displacement and DAFs of middle span slab

Profile	Speed m/s	Ud mm	DAF	Speed m/s	Ud mm	DAF
Perfect	10	-7.15	1.00	30	-7.28	1.02
Good	10	-7.40	1.04	30	-7.27	1.02
Poor	10	-7.49	1.05	30	-8.62	1.21
Perfect	20	-7.20	1.01	40	-7.90	1.11
Good	20	-7.33	1.03	40	-7.92	1.11
Poor	20	-7.51	1.05	40	-9.72	1.36

Table 3 DAFs of the arch and hanger on the key sections

Component	Location	1/4 span		Middle span		3/4 span	
Arch rib	Effect	$N$	$M$	$N$	$M$	$N$	$M$
	Positive value	-	1.27	-	1.51	-	1.31
	Negative value	1.24	1.19	1.15	1.19	1.13	1.35
Hanger	Effect	$N$	$\Delta\sigma$	$N$	$\Delta\sigma$	$N$	$\Delta\sigma$
	Positive value	1.13	1.23	1.05	1.14	1.15	1.30

bending moment, and axial force respectively. Traditionally DAFs values specified in codes for design of highway bridges have classically been derived from the measurement or simulation of global traffic action effects in the main structure elements of bridges, e.g. middle span slabs. And they are applied to the design of all members of the structure. However the dynamic effect of traffic actions on different members varies significantly. Even the DAFs of the same member, but derived from different action effects, may be different from each other. The local dynamic effect of individual member can be determined by local DAF. Since design of bridge members is based on their internal forces, it is necessary to calculate accurately the local DAFs of internal forces for the members.

In accordance with the definition of DAF, the dynamic displacements of middle span slab and corresponding DAFs under different vehicle speeds and road surface profiles are listed out in Table 2. If the displacement DAF of middle span slab is regarded as the global DAF for the whole bridge, its value is closely related to road surface roughness. Usually surface profiles of most highways can be classified as Good, then the DAFs calculated vary between 1.02 and 1.11. These values conform well to the specifications of 1.20 (OHBDC 1983), 1.15 (AASHTO 2005), 1.12 (AASHTO 2004) respectively, but are slightly higher than 1.05 (China code 2004). When the road surface roughness is Poor, the DAFs calculated vary between 1.05 and 1.36 which exceed the DAFs specified in the design codes by a large margin.

Table 3 summarizes the DAFs of the arch ribs and hangers in three key sections. The truck passes over the bridge with Good road at speed from 10 to 40 m/s. The effects including axial force  $N$ , bending moment  $M$ , and stress amplitude  $\Delta\sigma$  are applied to calculate the DAFs. It is shown that local DAFs on the key sections all exceed the global ones. The DAFs of the arch ribs derived from axial force differ significantly from those from bending moment with extreme discrepancy of 31% in middle span; The DAFs of the hangers derived from axial force and stress amplitude respectively are also considerably different with extreme discrepancy of 31% in 3/4 span.

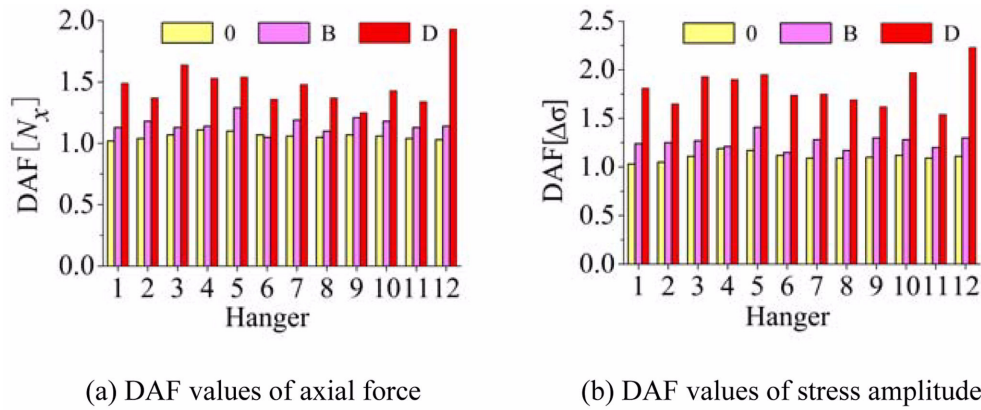


Fig. 6 Effects of road surface roughness on DAFs of the hangers

Fig. 6 shows the comparison of the DAF values of hangers under three road surface roughnesses. The DAF values of stress amplitude  $DAF[\Delta\sigma]$  vary between 1.14 and 1.30 which are much higher than the values of axial force  $DAF[N_x]$  1.05 to 1.15. And that the fatigue characteristics of the alloy under axial loading highly depend on the stress amplitude. Road surface roughness of a bridge seriously affects the local DAFs in hangers. The worse the bridge road condition, the larger the hangers' dynamic internal forces under truck load. In which the highest increases in hanger 12 (the shortest one) show that the side hangers are most susceptible to vehicular impact.

By comparison, the global DAFs are generally less than the local DAFs. Therefore it appears to be unreasonable to take into account the dynamic effect of traffic actions using a single global DAF. Local DAF should be chosen carefully according to the type of components and the action effects to be considered. When the road profile is Poor, the local DAFs increase at different extent depending on the type of components and the effects.

#### 4.3 Plane stress variation of the hangers

When the hangers are fixed at both ends, they are subjected to axial stress and bending stress simultaneously under passing vehicle. The maximum stresses  $\sigma$  on the perimeter of each hanger are a combination of the axial force  $N_x$  and the two bending moments  $M_z$  and  $M_y$ . Based on the plane section assumption, the stress variation in the plane can be defined by the Navier's equation as

$$\sigma = \frac{N_x}{A} \pm \frac{R}{I} \sqrt{M_z^2 + M_y^2} \cos(\theta - \varphi) \quad (11)$$

where  $R$  = radius of the hanger,  $A$  = area of the cross-section, = section moment of inertia ( $I = \pi R^4/4$ ),  $\varphi$  = angle between the resultant moment and longitudinal direction of the bridge ( $\varphi = \tan^{-1}(M_z/M_y)$ ).

The envelopes of the maximum tension and compression along the perimeter of hanger 1 and hanger 6 are shown in Fig. 7, where the radial axis shows the magnitude of the stress and the axis in the tangential direction shows the angle  $\varphi$ . The direction of vibration is best described by the angle of the largest mean stress along the perimeter. The maximum stresses on the perimeter of each hanger are a combination of the axial force and the two bending moments. Different hangers are subjected to different combinations of these forces. The shortest hangers have a small

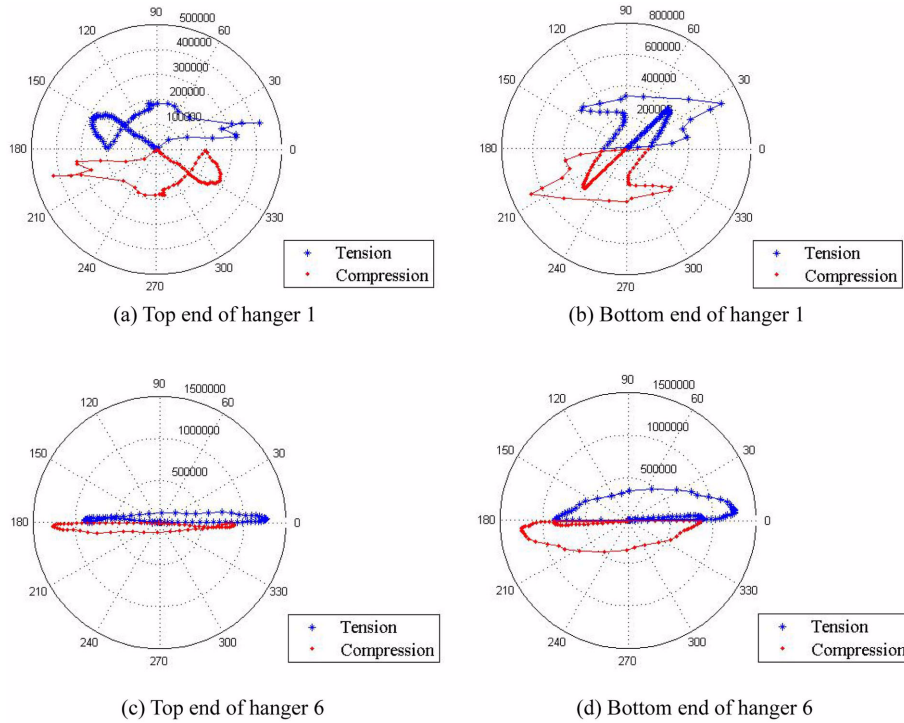


Fig. 7 Extreme stress variation on the perimeter of the hangers (Pa)

Table 4 Comparison of the maximum stress and axial stress in the hangers (Pa)

Hanger	Type	Top			Bottom		
		$\sigma$ (1)	$\sigma_{\max}$ (2)	Ratio (2)/(1)	$\sigma$ (3)	$\sigma_{\max}$ (4)	Ratio (4)/(3)
1#	Static	3.2889e7	3.3316e7	1.0130	3.2822e7	3.3173e7	1.0107
	Dynamic	3.7000e7	3.7300e7	1.0081	3.6900e7	3.7400e7	1.0136
	DAF	1.12	1.12	1.0000	1.12	1.13	1.0089
6#	Static	2.3156e7	2.3491e7	1.0145	2.2905e7	2.3363e7	1.0200
	Dynamic	2.4400e7	2.4700e7	1.0123	2.4200e7	2.4900e7	1.0289
	DAF	1.05	1.05	1.0000	1.06	1.07	1.0094

contribution of the moment  $M_y$  and a larger contribution of  $M_x$ , which means that they vibrate mainly in the transverse direction. In hanger 6,  $M_y$  is the largest moment and it mainly vibrates in longitudinal direction.

The maximum stresses in all hangers are mainly a result of the axial force as seen in Table 4. It should be noted that DAFs of hanger 1 are much higher than those of hanger 6 with higher absolute dynamic stresses.

#### 4.4 Acceleration response in frequency domain

After its acceleration time histories are transformed from time domain to frequency domain by

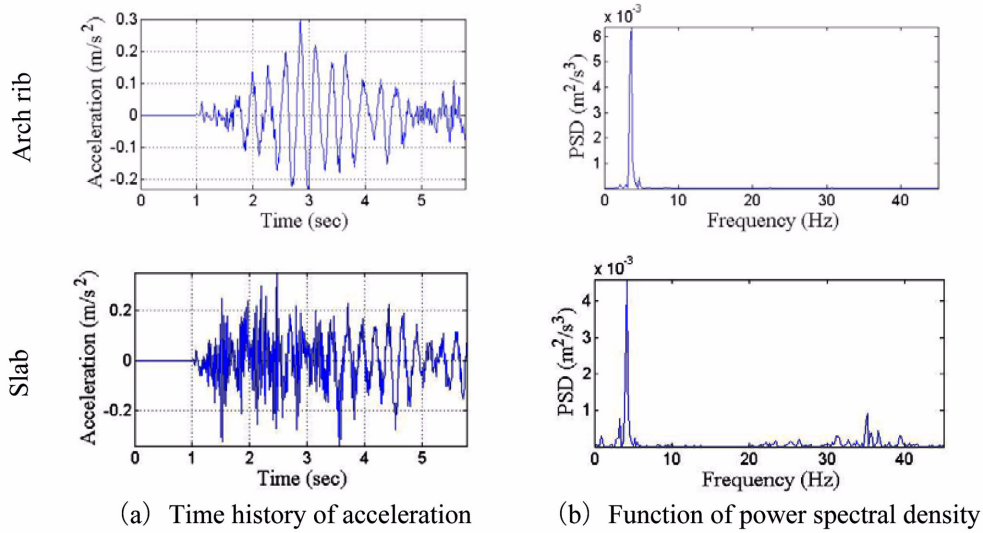


Fig. 8 Acceleration time history and power spectral density in middle span (Road surface profile = Perfect)

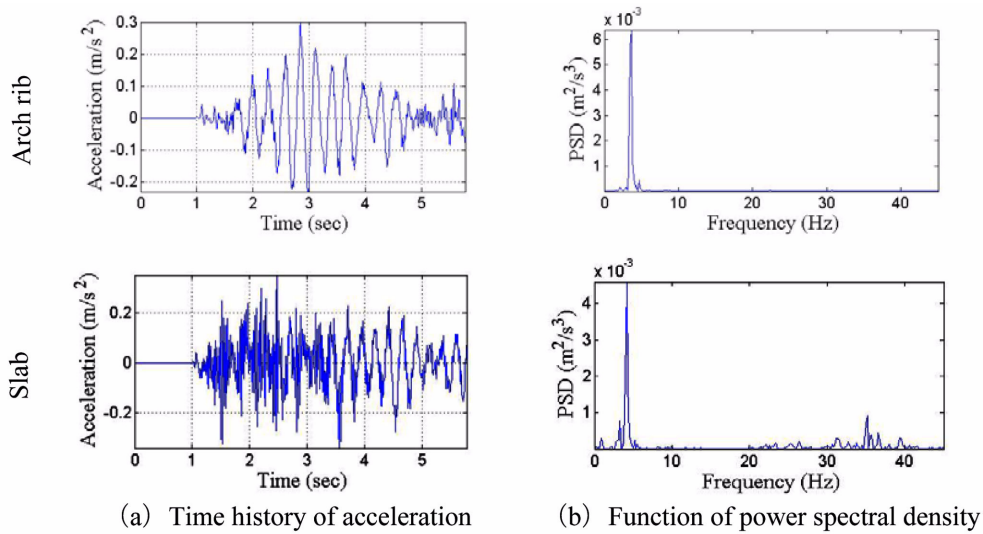


Fig. 9 Acceleration responses of hanger 1

fast Fourier transform (FFT), the performance of the bridge can also be clearly observed for the accelerations in the frequency domain. The time history and function of power spectral density (PSD) for the arch rib and slab in middle span are shown in Fig. 8.

The curves in time domain are quite different, but they have similar characteristics in frequency domain. For the arch rib, the peaks can be observed in frequencies of 0.8666 and 3.2932~3.4647 Hz, which are close to the 2nd, 10th and 11th vibration modes of the bridge, respectively. As to the slab, the peaks fall into frequencies of 0.8666 and 4.1590~4.3329 Hz, which are close to the 2nd and 13th modes, respectively. Both the arch rib and slab respond strongly in a frequency of 0.8666

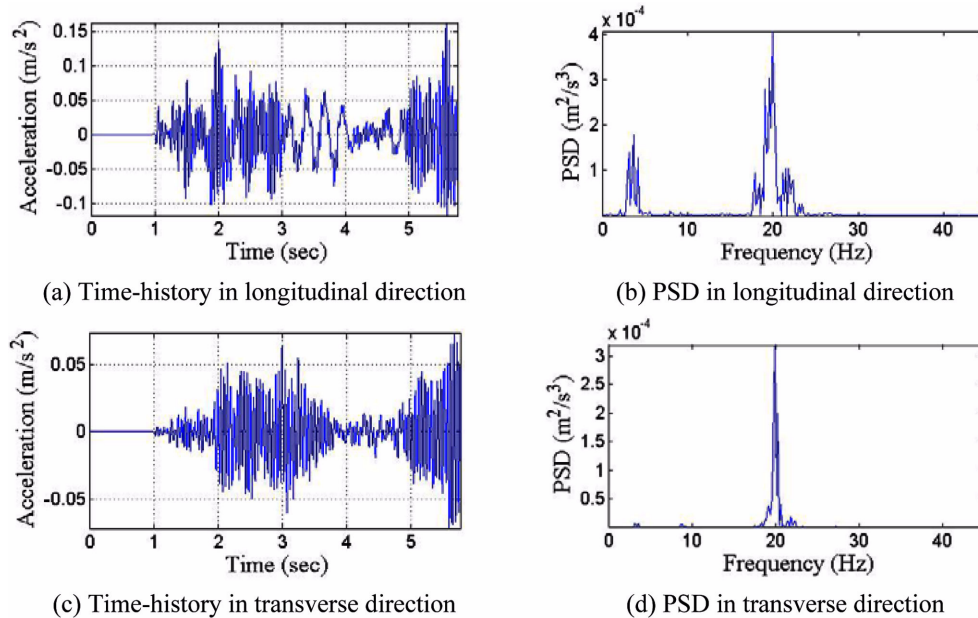


Fig. 10 Acceleration responses of hanger 6

Hz which is close, but not equal, to 0.9447 Hz (the second mode of the bridge), owing to the influence of vehicle mass.

Shown in Fig. 9 and Fig. 10 are, respectively, the acceleration response of hanger 1 and hanger 6 in time and frequency domain. All hangers vibrate primarily with their first natural frequencies. The peaks on the PSD curve are distributed in the frequency ranges of 18.1982 to 19.19325 Hz and 4.1596 to 6.2394 Hz, respectively, for hanger 1 (side hanger) and hanger 6 (middle span hanger). Along the PSD curves of longitudinal acceleration, peaks are observed at low frequencies. The reason for this is that the hangers vibrate simultaneously by itself and together with the whole bridge. When the road surface roughness is considered, some higher modes will be excited due to the intensified vibration of the vehicle.

## 5. Conclusions

Based on numerical simulation of vehicle-bridge interaction, this paper provides valuable information about the behavior and dynamic response of CFST tied-arch bridge under traveling vehicle. This information may be used to deduce DAFs for global and local vibrations. Based on the numerical results, the following conclusions can be drawn with respect to DAFs in CFST tied-arch bridge:

- Modal Coupled Method is proved to be efficient for the analysis of the interaction between vehicle and CFST tied-arch bridge. With the method the degree-of-freedom of the vehicle-bridge system can be remarkably reduced. Hence the computing efficiency of the algorithm is improved, and stability and accuracy are ensured at the same time.
- Road surface profile of the bridge seriously affects the vehicle vibrations, thus affecting the

vehicle-bridge interaction. Since the condition of road surface in the future is difficult to be estimated precisely during the design stage, it is necessary to refine the specification of design codes for DAFs considering different road surface conditions. This can also be done by specifying a minimum requirement for road surface conditions to use the DAFs of the current code specifications, especially for the maintenance and rating of existing bridges.

- c. Because the dynamic amplification factor is primarily used to amplify the internal static forces (axial force, moment, shear, etc.) in the design and evaluation of the bridge, it is therefore inappropriate to use the DAF calculated from the displacements, and it is more logical to amplify the internal forces and moments with the local DAF determined from the internal forces and reactions directly.
- d. Although the acceleration responses of arch ribs and hangers in time domain differ from each other, they have similar characteristics in frequency domain. The frequency response show that the hangers vibrate mainly in their first mode. Shorter hangers are more susceptible to the vehicular impact than the longer ones.
- e. Hangers play an important role as component of bearing intensive axial force. Though feature small size, they are composed of different parts and very sensitive to traffic loads. Large vibrations occur during vehicle passages, which could lead to fatigue failure. Thus special measures must be taken in design.

## Acknowledgements

This paper is supported by Funds for Applied Basic Research of Yunnan Province (2008ZC026M), and the Natural Science Foundation of Kunming University of Science and Technology (2008-044).

## References

- AASHTO (2005), *LRFD bridge design specifications*, American association of state highway and transportation officials, Washington (DC).
- AASHTO (2004), *Standard specifications for highway bridges*, American association of state highway and transportation officials, Washington (DC).
- Bhatt, P. (2002), *Programming the dynamic analysis of structures*, Spon Press, 11 New Fetter Lane, London EC4P 4EE.
- Chen, B.C. (2002), *Examples of CFST arch bridges*, China Communications Press, Beijing.
- Dodds, C.J. and Robson, J.D. (1973), "The description of road surface roughness", *J. Sound Vib.*, **31**(2), 175-183.
- Fafard, M., Laflamme, M., Savard, M. and Bennur, M. (1998), "Dynamic analysis of existing continuous bridge", *J. Bridge Eng.*, **3**(1), 28-37.
- Henchi, K., Fafard, M., Talbot, M. and Dhatt, G. (1998), "An efficient algorithm for dynamic analysis of bridges under moving vehicles using a coupled modal and physical components approach", *J. Sound Vib.*, **212**(4), 663-683.
- ISO (1995), *Mechanical vibration – Road surface profiles – Reporting of measured data*, ISO 8608: IDT, Geneva.
- Li, G.H. (1996), *Stability and vibration of bridge structures*, China Railway Publishing House, Beijing.
- Li, Q., Tian, X.M. and Zhang, Q.H. (2003), "A model test on long-span x-style tied arch bridge on railway", *China Railway Sci.*, **24**(1), 88-93.

- Lu, J.G. (2005), *Research on the damage of hangers of concrete-filled steel tubular arch bridges*, Tianjin, Tianjin University.
- Malm, R. and Andersson, A. (2006), "Field testing and simulation of dynamic properties of a tied arch railway bridge", *Eng. Struct.*, **28**, 143-152.
- Ontario Ministry of Transportation and Communication (1983), *Ontario highway bridge design code*, Ontario.
- Roeder, C.W., MacRae, G., Crocker, P., Arima, K. and Wong, S. (2000), "Dynamic response and fatigue of steel tied-arch bridge", *J. Bridge Eng.*, **5**(1), 14-21.
- Shan, D.S. and Li, Q. (2005), "Coupled vibration analysis of x-style arch bridge and vehicles", *J. Southwest Jiaotong Univ.*, **40**(1), 53-57.
- Song, Y.F., He, S.H. and Wu, X.P. (2001), "Energy method of the tension for fixed-end rigid cables", *J. Xi'an Highway Univ.*, **21**(1), 55-57.
- Trade Standard of People's Republic of China (2004), *JTG D60-2004 general code for design of highway bridges and culverts*, China Communications Press, Beijing.
- Wu, D.J., Wang, X.S. and Xiang, H.F. (2003), "The bridge-vehicle dynamics characteristic of Nelson arch bridge in high speed railway", *J. China Railway Soc.*, **25**(3), 96-100.
- Zhang, Y., Cai, C.S., Shi, X.M. and Wang, C. (2006), "Vehicle-induced dynamic performance of FRP versus concrete slab bridge", *J. Bridge Eng.*, **11**(4), 410-419.